Bio-Design and Manufacturing (2025) 8:724–741
https://doi.org/10.1631/bdm.2400390

RESEARCH ARTICLE

A hyaluronic acid-enhanced 3D-bioprinted osteosarcoma model reveals mechanisms of tumor metastasis and chemoresistance

Hangyu Zhou[1,2] · Miaoben Wu[1,2] · Zekai Ding[1] · Wei Su[3] · Hankang Jiang[1,2] · Kaixuan Chen[1,2] · Yibing Wu[3] · Enxing Yu[3] · Yuye Huang[1] · Qinghua Song[3] · Kailei Xu[1]

Received: 25 September 2024 / Accepted: 12 February 2025

Abstract

Osteosarcoma, an aggressive bone cancer found most often in children and adolescents, remains difficult to treat, and little improvement in survival rate has been observed over recent decades. The tumor microenvironment (TME), especially the extracellular matrix (ECM), is a critical factor determining cancer progression and chemotherapy resistance, yet traditional 2D models generally fail to replicate its properties. Recent development of 3D-bioprinted tumor models has facilitated improved simulation of the complexity of the TME, but specific models involving bioinks tailored to osteosarcoma remain underdeveloped. Gelatin methacryloyl (GelMA) is a common bioink that can rapidly gel and contains Arg-Gly-Asp (RGD) sequences. However, it lacks collagen's triple-helix structure that is essential for ECM–cell communication. Hyaluronic acid (HA) is a macromolecule that is aberrantly expressed in osteosarcoma by mechanisms that remain largely unexplored. In this study, we developed a composite bioink containing GelMA, collagen, and HA, and applied it to 3D bioprint an in vitro osteosarcoma model. We found that HA significantly enhanced osteosarcoma cell proliferation and chemoresistance, as well as the expression of epithelial–mesenchymal transition and cancer stem cell markers. Furthermore, we found that HA abundance was positively correlated with hypoxia and angiogenesis signaling pathways, and this occurred mainly via upregulation of hypoxia-inducible factor-1α (*HIF-1α*) and vascular endothelial growth factor A (*VEGFA*) expression, thereby contributing to increased chemoresistance. Overall, our study provides a protocol for building in vitro realistic 3D-bioprinted models for studying osteosarcoma, highlights the role of HA in osteosarcoma progression, and offers a platform for developing new chemotherapy treatments.

Hangyu Zhou, Miaoben Wu, and Zekai Ding have contributed equally to this work.

✉ Yuye Huang
huangyy63@mail2.sysu.edu.cn

✉ Qinghua Song
fyysongqinghua@nbu.edu.cn

✉ Kailei Xu
xukailei@zju.edu.cn

[1] Center for Medical and Engineering Innovation, The First Affiliated Hospital of Ningbo University, Ningbo 315010, China

[2] Health Science Center, Ningbo University, Ningbo 315211, China

[3] Department of Plastic and Reconstructive Surgery, The First Affiliated Hospital of Ningbo University, Ningbo 315010, China

Graphical abstract

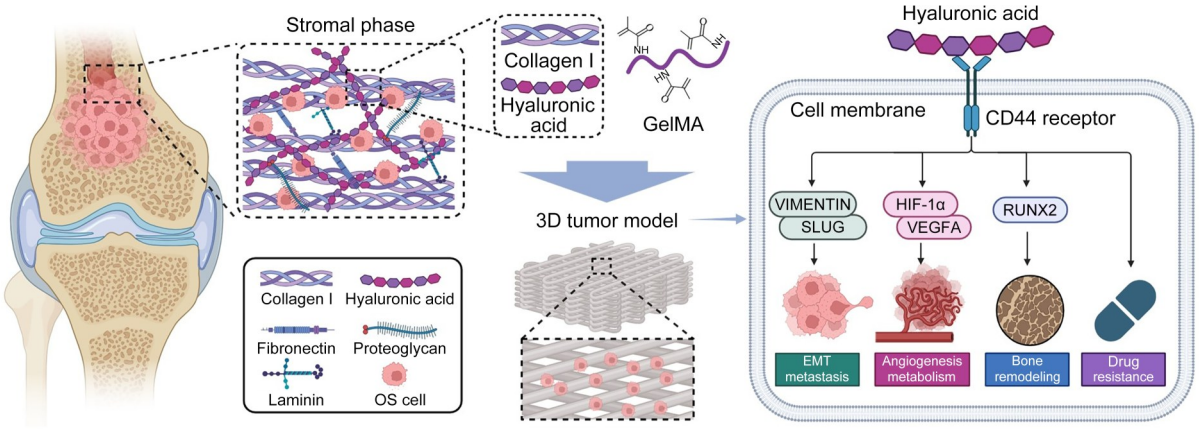

Keywords Bioinks · Cell-laden · Collagen · Gelatin methacryloyl (GelMA) · Hypoxia

1 Introduction

Osteosarcoma, the most prevalent primary malignant bone tumor in children and adolescents, typically arises in the metaphyseal regions of rapidly growing long bones, including the tibia and femur [1]. In general, osteosarcoma is characterized by the production of immature osteoids by tumor cells. Despite standard treatments of surgery and neoadjuvant chemotherapy, the five-year survival rate for osteosarcoma is approximately 60% [2], a figure that has not significantly improved over the past three decades. For patients with metastatic lesions, the prognosis is especially poor, with a five-year survival rate of less than 20% [3]. Thus, overcoming therapeutic resistance and preventing metastasis are critical challenges for the management of osteosarcoma.

The tumor microenvironment (TME) plays a crucial role in cancer progression and metastasis. The extracellular matrix (ECM), a key component of the TME, not only provides structural support for cells but also regulates cellular behaviors such as communication, proliferation, adhesion, migration, and differentiation, all of which are essential for osteosarcoma development [4]. In oncological research, conventional two-dimensional (2D) cell cultures, which lack components of the ECM, cannot replicate the complex architecture of osteosarcoma tissues. Moreover, despite the common usage of in vivo models, their use is often limited by ethical concerns and financial constraints [5]. Recent osteosarcoma research has facilitated the development of three-dimensional (3D) in vitro models that can better replicate the TME, including spheroids [6], porous hydrogels [7–9], and porous scaffolds [10]. In recent years, the rapid advancement of 3D bioprinting has also created a powerful platform for achieving patient-specific precision therapies. Unlike other common 3D culture methods, such as organoids and patient-derived xenografts, 3D bioprinting facilitates the production of in vitro tumor models and drug screening protocols due to its simplicity, low cost, and high stability. Previous studies from our lab have used 3D bioprinting to investigate cell–cell interactions in prostate cancer [11] and cell–ECM interactions in renal cell carcinoma [12]. Other research groups have also developed in vitro models of cholangiocarcinoma [13], hepatocellular carcinoma [14], and ovarian cancer [15] using 3D bioprinting, while others have assessed the effectiveness of antitumor drugs. However, to date, no studies have reported 3D bioprinting of osteosarcoma models, and no bioinks have been specifically designed to mimic the biological composition of the osteosarcoma ECM.

Among the ECM components within the osteosarcoma microenvironment, collagen and hyaluronic acid (HA) are particularly important. For example, elevated concentrations of collagen metabolites have been identified in the serum of untreated osteosarcoma patients, and supplementation with exogenous collagen has been shown to enhance the synthesis and activation of matrix metallopeptidase 2 (MMP2) in osteosarcoma cells, thereby facilitating the progression, invasion, and migration of osteosarcoma [16]. Similarly, HA (also known as hyaluronan or hyaluronate) is known to play a key role in the disease. As a macromolecule belonging to the glycosaminoglycan (GAG) family, HA is abundant in bone tissue and is aberrantly expressed in osteosarcoma, where it strongly correlates with cancer cell differentiation, proliferation, and migration [17, 18]. Moreover, inhibition of HA has been found to significantly reduce osteosarcoma cell viability

and induce apoptosis, and the underlying mechanisms responsible for these effects remain largely unexplored [19, 20].

In this study, we developed a gelatin methacryloyl (GelMA)-collagen-HA (GelMA-Col-HA) composite hydrogel that was used as a bioink for 3D bioprinting of an in vitro osteosarcoma model (Fig. 1). This hydrogel bioink was designed to more accurately replicate the interactions between cells and the ECM, with a particular focus on the effects of HA on cell behaviors. GelMA is a commonly used biomaterial due to its printability, rapid gelation, and mechanical properties; however, it lacks the unique triple-helix structure of collagen, a feature that is crucial for ECM−cell communication. Therefore, here we added collagen and HA to GelMA to better mimic the osteosarcoma ECM composition and improve hydrogel bioactivity. Moreover, material characterization of the composite bioink was conducted to evaluate the influence of collagen and HA on the printability and physical properties of GelMA. Finally, we conducted in vitro analysis in which MG63 cells were encapsulated in a bioink and bioprinted to investigate the influence of HA on various MG63 cellular behaviors.

2 Materials and methods

2.1 Materials

Gelatin (G108395) and methacrylic anhydride (MAA; M102519) were purchased from Aladdin Industrial (Shanghai, China). Matrigel (356234) was purchased from Corning (NY, USA). Collagen I (5005−100 mL, 3 mg/mL, bovine) was purchased from Advanced Biomatrix (Carlsbad, CA, USA). Methacrylated hyaluronic acid (HAMA; EFL-HAMA-400K), phenyl-2,4,6-trimethylbenzoylphosphinate (LAP; EFL-LAP), and GelMA lysis buffer (EFL-GM-LS-001) were purchased from Engineering For Life (Suzhou, China). MG63 was purchased from Procell (Shanghai, China), while the minimum essential medium (MEM; PM150410) was purchased from Pricella (Wuhan, China). Penicillin/Streptomycin (P/S; 15140122) and 0.25% trypsin–ethylenediaminetetraacetic acid (trypsin–EDTA, 25200056) were purchased from Gibco (Big Cabin, OK, USA). A cell counting kit-8 (CCK-8; C0038) was purchased from Beyotime (Shanghai, China). 4',6-Diamidino-2-phenylindole (DAPI; C0060), live/dead assay (CA1630), paraformaldehyde (PFA; P1110), phosphate-buffered saline (PBS; P1020), and phalloidin-fluorescein isothiocyanate (phalloidin-FITC, CA1640) were purchased from Solarbio (Beijing, China). All primers were synthesized by Sangon Biotech (Shanghai, China). TRIzol (15596018) and Power SYBR Green polymerase chain reaction (PCR) Master Mix (4367659) were purchased from Life (MA, USA). The FastKing gDNA dispelling reverse transcription (RT) supermix kit (KR118) was purchased from TIANGEN (Beijing, China). A bicinchoninic acid (BCA) protein assay kit was purchased from Thermo Fisher Scientific (MA, USA). Fetal bovine serum (FBS) was purchased from ExCell Bio (Shanghai, China). Cisplatin (CDDP; HY-17394) and Dox (ADM; HY-15142) were purchased from MCE (Shanghai, China). Primary antibodies against SLUG, VIMENTIN, TWIST, and CD44 were purchased from Cell Signaling Technology (MA, USA), while primary antibodies against NANOG and RUNX2 were purchased from Affinity (Jiangsu, China). In addition, the primary antibody against CD133 was purchased from ABclonal (Wuhan, China), and the primary antibodies against GAPDH and β-actin were purchased from Ray Antibody (Beijing, China). All secondary antibodies were purchased from Abcam (Cambridge, UK).

2.2 Synthesis of GelMA

For GelMA synthesis, we first added gelatin to a buffer solution containing Na_2CO_3 (174.4 mmol/L) and $NaHCO_3$ (75.0 mmol/L). This mixture was then stirred at 50 °C for 2 h until completely dissolved. Subsequently, 0.6% (volume

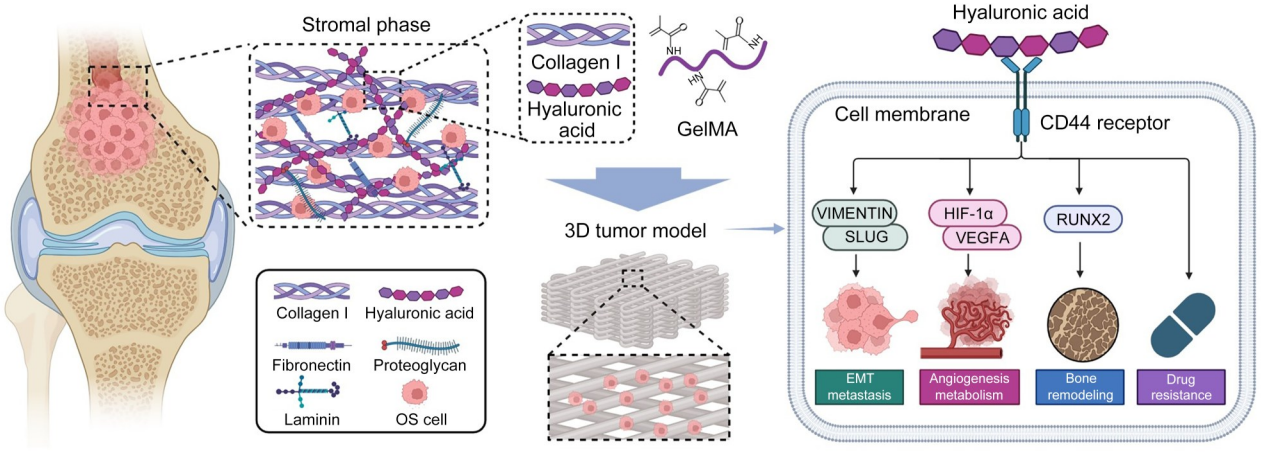

Fig. 1 Schematic diagram of the GelMA-Col-HA composite hydrogel for a 3D-bioprinted in vitro osteosarcoma model. OS: osteosarcoma

fraction) methacrylic acid was incorporated into the gelatin solution and stirred at 50 °C for another 2 h in dark conditions. The resulting mixture was diluted with ultrapure water in a 1:9 ratio after being dialyzed at room temperature for three days, during which the water was changed three times per day. Ultimately, all samples were lyophilized and stored at 20 °C until subsequent use.

The degree of methacrylation substitution for GelMA made in the above conditions was determined using a 2,4,6-trinitrobenzenesulfonic acid (TNBS) assay with all protocols performed using a previously published method [21]. Briefly, GelMA and gelatin powder were separately dissolved in 0.1 mol/L sodium bicarbonate buffer at a concentration of 1.6 mg/mL. Next, 500 μL of each sample was mixed with 500 μL of 0.1% TNBS solution, and the resulting mixture was incubated at 37 °C for 2 h. The reaction was stopped by adding 250 μL of 1 mol/L hydrochloric acid and 500 μL of 10% (0.1 g/mL) sodium dodecyl sulfate solution. The absorbance values of all samples were measured at 335 nm, and the molar concentration of free primary amino groups present in the samples was determined by comparing the measured absorbance values to a standard curve generated from glycine solutions with concentrations of 0, 6.75, 12.5, 25, 50, and 100 μg/mL. Using this method, the degree of methacrylation substitution for GelMA made in the above conditions was 50%.

2.3 Hydrogel preparation

To create hydrogels, varying concentrations of GelMA (i.e., 5%, 7.5%, 10%, and 15% (0.05, 0.075, 0.10, and 0.15 g/mL)) were dissolved at 37 °C in a fully supplemented cell culture medium containing 0.5% LAP as a photoinitiator. Precursors were then sterilized using a 0.22-μm filter for cell cultures. For collagen, eight parts of collagen I stock solution were combined with one part of 10× Dulbecco's modified Eagle's medium (DMEM) solution on ice and then neutralized with a sterile NaOH solution. Next, the collagen solution was mixed with GelMA at room temperature to produce precursors. These had a constant GelMA concentration (5%, mass fraction) and different collagen concentrations as follows: 5% GelMA-0.08% (mass fraction) Col, 5% GelMA-0.12% (mass fraction) Col, and 5% GelMA-0.16% (mass fraction) Col. In addition, different compositions of HAMA were dissolved at 37 °C in a fully supplemented cell culture medium containing 0.5% LAP. This was then added to GelMA-Col solutions at room temperature to produce the following GelMA-Col-HA precursors: 5% GelMA-0.16% Col-0.1% HA and 5% GelMA-0.16% Col-0.5% HA.

2.4 Compression assays

Next, we performed compression tests (n=3 per group) to analyze the compressive modulus for all groups. To do so, we used a mechanical testing instrument (AGS-X, Shimadzu, Japan) and performed all tests at room temperature. Hydrogel samples were produced in a cylinder shape with a thickness of 2 mm and a diameter of 8 mm. The compressive modulus was calculated from the slope of the linear region (i.e., 0% to 30% strain) on the stress–strain curve.

2.5 Swelling tests

For the GelMA-0.08% Col, GelMA-0.12% Col, and GelMA-0.16% Col samples, precursors were produced in a cylinder shape with 2 mm thickness and 8 mm diameter (n=3 per group) before being submerged in water, PBS, and fully supplemented cell culture medium, and then incubated at 37 °C with 5% CO_2 for five days. For the GelMA-0.16% Col, GelMA-0.16% Col-0.1% HA, and GelMA-0.16% Col-0.5% HA samples, precursors were first mixed with MG63 cells, printed to a grid structure, submerged in a fully supplemented cell culture medium, and then incubated at 37 °C with 5% CO_2 for five days. Measurements of sample diameter or edge length were taken using a digital caliper (Deli, Ningbo, China) at predetermined time points, i.e., 0, 0.5, 1.5, 4, 6, 24, 48, 72, and 120 h. The diameters or edge lengths obtained were then normalized to an initial measurement at 0 h to determine the hydrogel swelling rate.

2.6 Scanning electron microscopy (SEM)

SEM (Phenom Pro, the Netherlands) was used to investigate the pore architecture of hydrogels with varying compositions (n=3 per group). All samples were subjected to a 24-h freeze-drying treatment using a vacuum chamber (DYYB-10, Shanghai Deyangyibang Instruments Co., Ltd., Shanghai, China). Dried samples were then sputtered and coated with gold using an ion sputtering device (ISC 150, Supro Instruments, NY, USA), and the pore structure was imaged at multiple sites for each sample.

2.7 Rheology analysis

The rheological behaviors of all precursor solutions (n=3 per group) were evaluated using a HAAKE MARS iQ Air Rheometer (Thermo Fisher Scientific) using a plate geometry with a diameter of 25 mm for all measurements. Next, we explored viscosity changes at various temperatures between 4 and 35 °C using a steady shear rate of 10 s^{-1}. Subsequently, the storage modulus (G') and loss modulus (G'') were subjected to a uniform shear stress of 1 Pa and a frequency of 1 Hz for the same duration.

2.8 Filament fusion test

Next, we evaluated the effect of collagen and HA on GelMA printability using filament fusion tests, with all procedures

following a previously published method [12]. For all tests, we used a square pattern with increasing filament-to-filament distance (i.e., ranging from 1.5 to 4.0 mm with 0.5 mm increments; n=5 per group). All bioink compositions were printed at 20 °C and imaged immediately. The diffusion rate (r_{Df}) was calculated using the following equation:

$$r_{Df} = \frac{A_t - A_a}{A_a} \times 100\%, \quad (1)$$

where A_t represents the theoretical area of all pores and A_a is the actual total pore area. A_a was determined using image analysis performed with NIH ImageJ software. For an ideal square pore, r_{Df} should be 0 and A_t=A_a, indicating that no material spreading is taking place.

2.9 Uniformity factor analysis

A uniformity factor (U) was used to assess how closely printed strands resembled a theoretically perfectly uniform strand. To do so, all bioink compositions were first printed at 20 °C (n=3 per group) and imaged immediately. Next, the outer edge of both sides of the strand was outlined and measured using ImageJ. The length of the measured strand was then divided by the length of a perfectly uniform strand to calculate its uniformity factor. Here, values greater than 1 (U>1) indicated nonuniformity, while a value of 1 (U=1) indicated a perfectly uniform strand.

2.10 3D bioprinting of an in vitro osteosarcoma model

We next tested bioprinting of an in vitro osteosarcoma model. To do so, we cultured MG63 cells with MEM enriched with 10% (volume fraction) FBS and 1% (volume fraction) P/S. The culture medium was changed every other day. After reaching 80%–90% cellular confluency, MG63 cells were detached via 0.25% trypsin-EDTA. This was followed by centrifugation at 1000 r/min for 3 min and then subsequent resuspension in the respective precursor solution (i.e., 5% GelMA-0.16% Col, 5% GelMA-0.16% Col-0.1% HA, or 5% GelMA-0.16% Col-0.5% HA) until the cells reached a density of 2×10^6 cells/mL. The cellular density of osteosarcoma tissue is around 1×10^7 cells/mL, and it comprises not only cancer cells but also stromal cells such as osteoblasts, osteoclasts, and immune cells [22]. Consequently, the density of cancer cells alone is likely lower than 1×10^7 cells/mL; thus, most in vitro osteosarcoma models use cellular density values between 1×10^4 to 1×10^6 cells/mL [8, 22–25]. An LB119 3D cellular bioprinter (Medprin, China) was used to construct in vitro osteosarcoma models. Briefly, the cell/precursor mixture was pumped into a sterile syringe equipped with a 24G needle to print a 6 mm×6 mm×2 mm grid structure (Fig. S1 in the supplementary information). After crosslinking under 405-nm ultraviolet (UV) light for 30 s, all constructs were transferred to 24-well tissue culture plates and incubated at 37 °C with 5% CO_2.

2.11 MG63 encapsulation in Matrigel and collagen

Next, we performed encapsulation of MG63 cells. To do so, we first prepared a collagen solution by combining eight parts of a type I collagen stock solution with one part of 10× DMEM solution in a 50 mL centrifuge tube on ice. This mixture was then neutralized using 0.05 mol/L sterile NaOH. When MG63 cells reached 70% confluence, they were detached using 0.25% trypsin-EDTA, washed, and resuspended in either collagen or Matrigel solution at a final density of 2×10^6 cells/mL. These cell suspensions were immediately added to 48-well plates and incubated at 37 °C for 2 h to facilitate gel solidification. During incubation, the culture medium was replaced every second day.

2.12 CCK-8 assays

On Days 1, 3, 5, and 7 of the incubation period, we performed CCK-8 assays to evaluate the proliferation rate of MG63 cells. These assays were performed for all samples with all procedures following the manufacturer's protocol. Briefly, 3D-bioprinted samples (n=3 per group) were transferred to a new 24-well plate. Each well was then supplemented with 350 μL of fully supplemented cell culture medium containing 10% (volume fraction) CCK-8 reagent and then incubated at 37 °C for 90 min. After incubation, 100 μL of CCK-8 mixture from each well was transferred to a 96-well plate to obtain fluorescence readings at 450 nm. Cell proliferation rates at the above-named intervals were normalized against the initial absorbance measured on Day 1.

2.13 Live/Dead assays

Next, we performed live/dead assays to determine the cellular viability of MG63 cells in the GelMA-0.16% Col, GelMA-0.16% Col-0.1% HA, and GelMA-0.16% Col-0.5% HA samples after bioprinting on Day 3. For these assays, all procedures followed the manufacturer's protocol. Specimens (n=3 per group) were first washed three times with assay buffer, and then exposed to 500 μL of working solution for 15 min in an incubator. After incubation, they were washed with assay buffer again before being imaged under a fluorescence microscope (Leica Microsystems, Germany).

2.14 Phalloidin staining

For phalloidin staining, we subsampled each 3D-bioprinted sample (n=3 per group) on Days 1, 3, 5, and 7 of incubation.

Cells from these samples were first fixed with 4% paraformaldehyde, washed three times with PBS, and then permeabilized with 0.5% Triton X-100 at room temperature for 30 min. Next, they were incubated with phalloidin solution (1:200) for 90 min and then with DAPI for 20 min, and finally imaged using a confocal microscope (Nexcope, Ningbo, China).

2.15 Immunofluorescence staining

For immunofluorescence staining, we obtained 3D-bioprinted samples (n=3 per group) on Day 5 of incubation. Cells were first fixed with 4% paraformaldehyde before being washed with PBS three times, permeabilized with 0.5% Triton X-100 at room temperature for 30 min, and then blocked with 5% bovine serum albumin (BSA) for 1 h. Samples were then incubated overnight at 4 °C with a primary antibody, including RUNX2 (1:500), CD133 (1:200), VIMENTIN (1:200), TWIST (1:500), and NANOG (1:500). Samples were then stained for 90 min at room temperature with a goat anti-rabbit immunoglobulin G (IgG; 1:500) secondary antibody, after which cell nuclei were stained with DAPI. Finally, cell imaging was performed using a confocal microscope (Nexcope), and fluorescence intensity was quantified using NIH ImageJ.

2.16 RNA extraction

Total RNA was extracted using TRIzol (Life), and then subjected to chloroform phase separation, precipitation by isopropanol, two rounds of washing with 75% ethanol, and a final dilution in RNase-free water. RNA concentrations were measured using a Nanodrop spectrophotometer (Thermo Fisher Scientific).

2.17 RNA-seq and data analysis

RNA integrity was evaluated using an Agilent 2100 Bioanalyzer (Agilent Technologies, CA, USA). Library construction was performed using a VAHTS Universal V6 RNA-seq Library Prep Kit, with all procedures following the manufacturer's protocol. OE Biotech Co., Ltd (Shanghai, China) performed transcriptome sequencing and analysis. Sequencing was conducted on an Illumina NovaSeq 6000 platform and produced 150-base-pair (150-bp) paired-end reads. On average, 50 million raw reads were generated per sample. The initial processing of raw reads (fast quality (FASTQ) formatted) was performed using FASTQ to remove low-quality sequences, thereby yielding clean reads for downstream analysis. These reads were subsequently aligned to the reference genome via hierarchical indexing for spliced alignment of transcripts 2 (HISAT2). Gene expression levels were quantified as fragments per kilobase million (FPKM), and read counts were determined using HTSeq-count. Sample reproducibility was assessed using principal component analysis (PCA) implemented in R version 3.2.0. DESeq2 was used to conduct differential expression analysis, with a Q value of <0.05 and a fold change of >2 or <0.5 taken as the operational definition of significantly differentially expressed genes (DEGs). Hierarchical clustering mapped gene expression patterns across various groups and samples. Furthermore, Gene Ontology (GO) pathway enrichment analysis of all DEGs, using a hypergeometric distribution, identified significantly enriched GO terms. Visualization of these analyses, including column, chord, and bubble diagrams, was also performed in R version 3.2.0. Finally, we employed gene set enrichment analysis (GSEA), using a predefined gene set, to rank genes by differential expression between sample types and assessed enrichment at the extremes of the ranked list.

2.18 Real-time polymerase chain reaction (PCR)

Complementary DNA (cDNA) was synthesized using extracted RNA and the FastKing DNA Dispelling RT SuperMix kit, with all procedures following the manufacturer's instructions. Relative gene expression was analyzed via real-time PCR (Roche, Basel, Switzerland). A mixture of Power SYBR Green PCR Master Mix, 20 ng of cDNA, and specific primers was prepared in 10 μL total reaction volume (n=3 wells per primer).

2.19 Western blotting

On Day 5 of incubation, we collected 3D-bioprinted samples (n=3 per group) from each experimental condition. Cells from these samples were lysed using ice-cold radioimmunoprecipitation assay (RIPA) buffer for 30 min, followed by centrifugation at 12 000 r/min for another 30 min. We then collected the supernatant and measured the protein concentrations using a BCA protein assay kit, which employed BSA (0.5 mg/mL) as a standard. Subsequently, 20 μg of total protein from each group was subjected to polyacrylamide gel electrophoresis. Protein samples were then transferred to polyvinylidene fluoride membranes, blocked with nonfat milk at room temperature for 2 h, and then incubated overnight at 4 °C with a primary antibody, such as rabbit anti-human GAPDH (1:10 000), β-actin (1:10 000), CD44 (1:1000), CD133 (1:1000), TWIST (1:1000), SLUG (1:1000), or VIMENTIN (1:1000). After overnight incubation, membranes were incubated again with horseradish peroxidase (HRP)-linked goat anti-rabbit and goat anti-mouse secondary antibodies (1:5000) for 1 h at room temperature. Visualization was performed using a Clarity western enhanced chemiluminescence (ECL) substrate (BIO-RAD, CA, USA),

and quantification of western blotting results was performed using NIH ImageJ.

2.20 Cell scratch assays

On Day 5 of incubation, we obtained MG63-laden samples from each experimental condition and submerged them in lysis buffer for 3 h to release cells. These were subsequently collected and plated in 24-well plates (n=3 per group). Once the cells reached 95%–100% confluence, a scratch was introduced in the center of each cell culture well using a pipette tip. The scratched area was imaged daily from Day 0 to Day 2 using an inverted microscope (Leica Microsystems). Wound closure was calculated by dividing the wound area without cells at each time point by the wound area measured on Day 0.

2.21 Drug responses

Next, a drug resistance test was performed for all 3D-bioprinted samples at Day 4 (n=3 per group). To do so, ADM and CDDP were added to fully supplemented media, and cell viability was evaluated after 24, 48, and 72 h of drug exposure using CCK-8 assays. Cell viability was calculated by evaluating sample absorbance relative to vehicle absorbance for all groups.

2.22 Statistical analyses

All statistical results were analyzed using GraphPad Prism version 8.02, unless specified otherwise. Each experiment was conducted using three biological replicates, and all data are presented as mean±standard deviation. Student's t-tests and analyses of variance (ANOVAs) were used to determine the statistical significance of differences in group means. For all tests, a p-value of 0.05 was considered to be statistically significant. Significance levels are denoted as $^{*}p<0.05$, $^{**}p<0.01$, and $^{***}p<0.001$.

3 Results

3.1 GelMA-Col hydrogel mimics the composition of the ECM in osteosarcoma

In this study, we incorporated various compositions of pure collagen into GelMA to improve its bioactivity. The appearances of the precursor solutions, including GelMA, GelMA-0.08% Col, GelMA-0.12% Col, and GelMA-0.16% Col, are shown in Fig. S2a (supplementary information). This figure shows that the inclusion of collagen increased the precursor viscosity. This trend was further verified via rheological analysis, in which the viscosity of the precursor solutions increased significantly with increasing collagen concentration under various temperatures at a constant shear rate (Fig. 2a). The storage and loss moduli of precursor solutions were also measured under various temperatures (Fig. 2b). We found that all compositions could undergo gelation at approximately 30 °C, indicating that collagen did not influence GelMA gelation. Hydrogel stability was further analyzed via swelling tests in fully supplemented MEM media, PBS, and water at 37 °C. These results showed that all hydrogel compositions exhibited a low swelling rate and remained stable throughout the testing (Figs. S2b–S2d in the supplementary information).

Next, MG63 cells were cultured in all GelMA-Col hydrogel compositions to evaluate the influence of collagen on MG63 cellular behavior and to identify the optimal collagen composition for subsequent experiments. Cellular proliferation rates were analyzed using CCK-8 assays, and we found that all hydrogel compositions could successfully support cellular growth throughout the culturing (Fig. 2c). Moreover, cells in the GelMA-0.16% Col group demonstrated the highest proliferation rate at Days 5 and 7, indicating that collagen can promote osteosarcoma growth. Cellular morphology was analyzed using phalloidin staining from Day 1 to Day 7. We found that MG63 cells formed cellular spheroids in all compositions of the hydrogel (Fig. S2e in the supplementary information). Moreover, in hydrogels containing collagen, cells began to show an elongated morphology by Day 3, and a similar phenomenon was observed until Day 5 for GelMA-only samples.

Next, we analyzed the expression of epithelial–mesenchymal transition (EMT)-related genes (i.e., *TWIST*, *VIMENTIN*, *CD44*, *MMP9*, *MMP13*, and *EPCAM*), cancer stem cell (CSC)-related genes (i.e., *OCT4* and *CD133*), and osteogenesis-related genes (i.e., *RUNX2*, *SPP1*, *PTHLH*, and *IBSP*) via quantitative reverse transcription polymerase chain reaction (qRT-PCR). We found that MG63 cells in the GelMA-Col hydrogel had significantly higher levels of overall gene expression relative to the GelMA sample (Figs. S2f–S2q in the supplementary information), suggesting that collagen can promote MG63 stemness and metastasis. Next, we analyzed MG63 cell protein expression via immunofluorescence staining and western blotting (Figs. 2d–2l). We found that VIMENTIN, CD133, SLUG, and RUNX2 all showed their highest levels of expression in the GelMA-0.16% Col hydrogel. Overall, based on material characterization and biological analysis data, we selected the GelMA-0.16% Col hydrogel for subsequent experiments.

3.2 Material characterization of GelMA-Col-HA bioinks

To better mimic the ECM composition of the osteosarcoma microenvironment, we added various concentrations of HA to the GelMA-0.16% Col hydrogel. The appearances of precursor

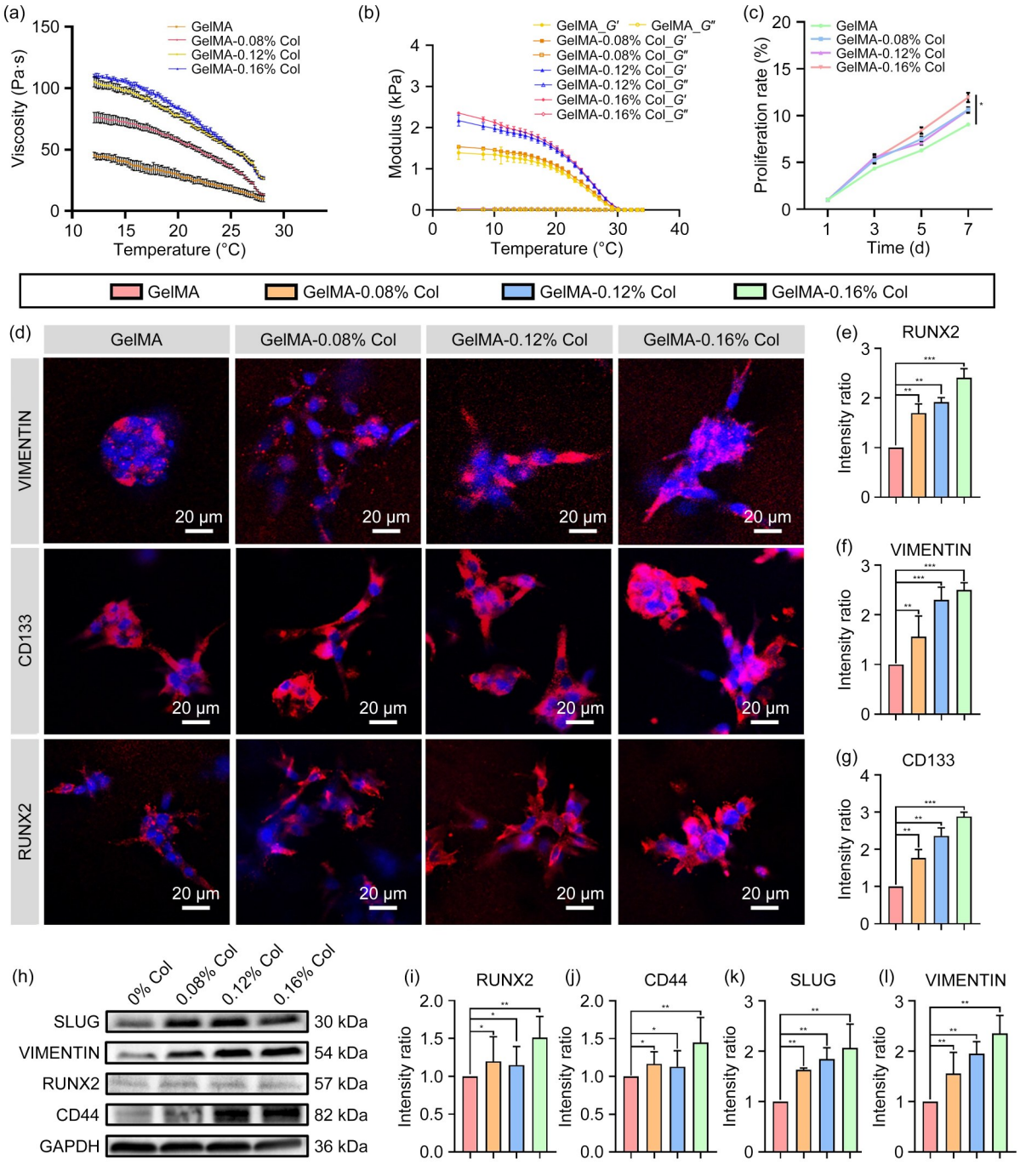

Fig. 2 Material characterization and biological analysis of GelMA-Col samples: (a) viscosities of precursors at various temperatures; (b) temperature conditions for precursor storage and loss moduli; (c) cellular proliferation rates in GelMA-Col; (d) immunofluorescence images for VIMENTIN, CD133, and RUNX2; (e–g) semi-quantification analysis of RUNX2, VIMENTIN, and CD133 proteins in immunofluorescence staining; (h) western blotting results for SLUG, VIMENTIN, RUNX2, and CD44; (i–l) semi-quantification analysis of RUNX2, CD44, SLUG, and VIMENTIN proteins in western blotting. Data are expressed as mean±standard deviation (n=3); $^{*}p<0.05$, $^{**}p<0.01$, and $^{***}p<0.001$

solutions, including GelMA-0.16% Col, GelMA-0.16% Col-0.1% HA, and GelMA-0.16% Col-0.5% HA, are shown in Fig. 3a. We found no significant differences in viscosity following the inclusion of HA; this result was verified by rheological analysis (Fig. 3b). Next, we determined the storage and loss moduli of all precursor solutions (Fig. 3c), and found that the inclusion of HA significantly increased the storage modulus, while the gelation temperature remained close to 30 °C. The hydrogel surface structure was then imaged via SEM (Fig. 3d), revealing that all samples had interconnected pore structures and that they did not display significant differences in pore size. Hydrogel stability was further analyzed

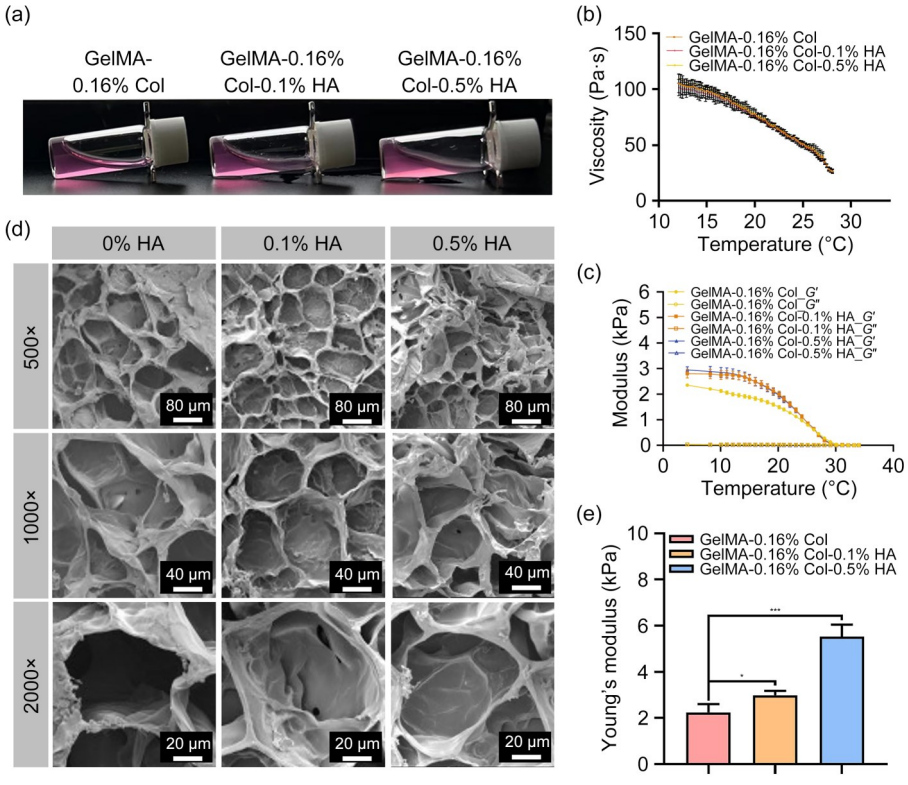

Fig. 3 Material characterization of GelMA-Col-HA samples: (a) appearances of GelMA-Col-HA precursors; (b) viscosities of precursors at various temperatures; (c) temperature conditions for precursor storage modulus and loss modulus tests; (d) surface structure of the GelMA-Col-HA hydrogel; (e) hydrogel compressive modulus. Data are expressed as mean±standard deviation (n=3); $^{*}p<0.05$ and $^{***}p<0.001$

with cell-laden printed structures; here we found that all compositions were stable at Day 5 and that cells had limited influence on the grid structure (Figs. S3a and S3b in the supplementary information). Furthermore, the inclusion of HA significantly increased the compressive modulus of the hydrogel (Fig. 3e), which still remained within the range of the Young's modulus of bone marrow (i.e., 0.25–15.7 kPa) [26, 27].

3.3 Printability analysis of GelMA-Col-HA composite bioinks

To further analyze the influence of collagen and HA on the properties of GelMA, we assessed the printability of all bioink compositions. For this test, all bioinks were printed with designated patterns to determine how composition affected pore closure and filament fusion (Fig. 4a); we also quantified the diffusion rate of each bioink (Fig. 4d). Our results showed that the inclusion of collagen slightly increased the diffusion rate, while the addition of HA improved printability. Next, we examined the uniformity factor for all bioinks (Fig. 4b). As in the filament fusion test, the GelMA-0.16% Col group had a higher uniformity factor than the other groups (Figs. 4c and 4e), indicating that it had more non-uniform strands. In addition, the inclusion of HA could reduce the uniformity factor closer to 1.

Subsequently, we used the GelMA, GelMA-Col, and GelMA-Col-HA bioinks to print more complicated structures to evaluate their relative printability. These structures included a 5-layered Chinese knot with a size of about 10.5 mm×10.5 mm×1.0 mm (wall thickness: 0.4 mm), a 15-layered thin-wall hollow tube with a diameter of about 3.5 mm and a height of 10 mm (wall thickness: 0.4 mm), a 5-layered snowflake with a size of about 16 mm×16 mm×1 mm (wall thickness: 1 mm), and a set of letters ("NBU") with a size of about 30 mm×8 mm×1 mm (7.5 mm×8.0 mm×1.0 mm each). The side, top, and zoomed-in views of all these structures are shown in Fig. 5.

3.4 MG63 cells had distinct transcriptional profiles among the GelMA-Col-HA bioinks

Global transcriptome profiling was performed using RNA sequencing (RNAseq) of MG63 cells bioprinted in GelMA-0.16% Col, GelMA-0.16% Col-0.1% HA, and GelMA-0.16% Col-0.5% HA bioinks to investigate the impact of HA on the transcriptional signatures of osteosarcoma cells. PCA revealed that MG63 cells subjected to HA stimulation showed distinct and different transcriptional profiles relative to control samples. For example, for MG63 cells in the GelMA-0.16% Col-0.1% HA bioink, we found that several cancer-related

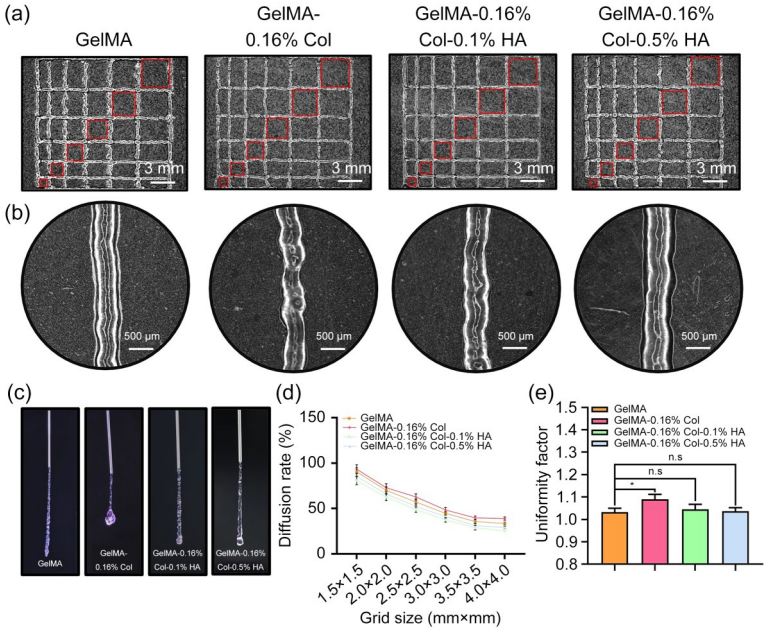

Fig. 4 Printability analysis of GelMA-Col-HA bioinks: (a) filament fusion test of bioinks; (b) uniformity factor analysis of bioinks; (c) images of bioink strand formation; (d) quantification of the filament fusion test results; (e) quantification of uniformity factor analysis. Data are expressed as mean±standard deviation (n=3); $^{*}p<0.05$; n.s.: not significant

or prognostic genes were significantly upregulated in response to HA stimulation; these included *ZEB1*, *ITGB2*, and *WNT4* (Fig. 6a). Similar results were found for cells in the GelMA-0.16% Col-0.5% HA bioink (Fig. S4a in the supplementary information).

Next, GO enrichment analysis on the RNAseq dataset was performed to investigate the changes in biological processes, cellular components, and molecular functions of MG63 cells under HA stimulation. For MG63 cells in the GelMA-0.16% Col-0.1% HA bioink (Fig. 6b), the enriched GO terms identified were involved in biological processes such as bone mineralization, cell–cell adhesion, and positive regulation of cell migration. Moreover, the enriched GO terms involved in molecular functions included MAP kinase activity, CCR2 chemokine receptor binding, and CCR3 chemokine receptor binding. Next, for MG63 cells in GelMA-0.16% Col-0.5% HA bioink (Fig. S4b in the supplementary information), the enriched GO terms involved in biological processes included regulation of cell–substrate adhesion, regulation of bone development, and inflammatory response. Furthermore, the enriched GO terms involved in molecular functions included CCR chemokine receptor binding, hyaluronic acid binding, and chemokine activity. Taken together, these results indicated that MG63 cells under HA stimulation may have higher chemokine activity.

Next, we performed a Kyoto Encyclopedia of Genes and Genomes (KEGG) enrichment analysis on the same enrichment dataset. For MG63 cells in the GelMA-0.16% Col-0.1% HA bioink (Fig. 6c), enriched gene sets were found to be involved in the VEGF signaling pathway, Rap1 signaling pathway, chemokine signaling pathway, and cAMP signaling pathway. Similar results were found for MG63 cells in the GelMA-0.16% Col-0.5% HA bioink (Fig. S4c in the supplementary information), whose enriched gene sets included the VEGF signaling pathway, PPAR signaling pathway, and chemokine signaling pathway. Moreover, each of these gene sets had positive correlations with cancer cell proliferation, migration, invasion, and drug resistance.

The HIF-1α signaling pathway was further evaluated using a heat map analysis (Fig. 6d) since it is closely associated with osteosarcoma progression, angiogenesis, and metastasis. For MG63 cells in the GelMA-0.16% Col-0.1% HA and GelMA-0.16% Col-0.5% HA bioinks, the HIF-1α signaling pathway was found to be more highly activated compared to cells in the GelMA-0.16% Col bioink. Interestingly, cells in the GelMA-0.16% Col-0.1% HA bioink showed higher levels of gene expression of *HIF-1α* compared with those in the GelMA-0.16% Col-0.5% HA bioink. These results were further verified by PCR, where we found that cells in the GelMA-0.16% Col-0.1% HA bioink showed higher levels of gene expression of *HIF-1α* and *VEGFA* compared to the other two groups (Figs. S3c and S3d in the supplementary information).

3.5 Influence of HA on osteosarcoma cell behavior

The proliferation rates of MG63 cells bioprinted in the GelMA-0.16% Col, GelMA-0.16% Col-0.1% HA, and GelMA-0.16% Col-0.5% HA bioinks were analyzed using

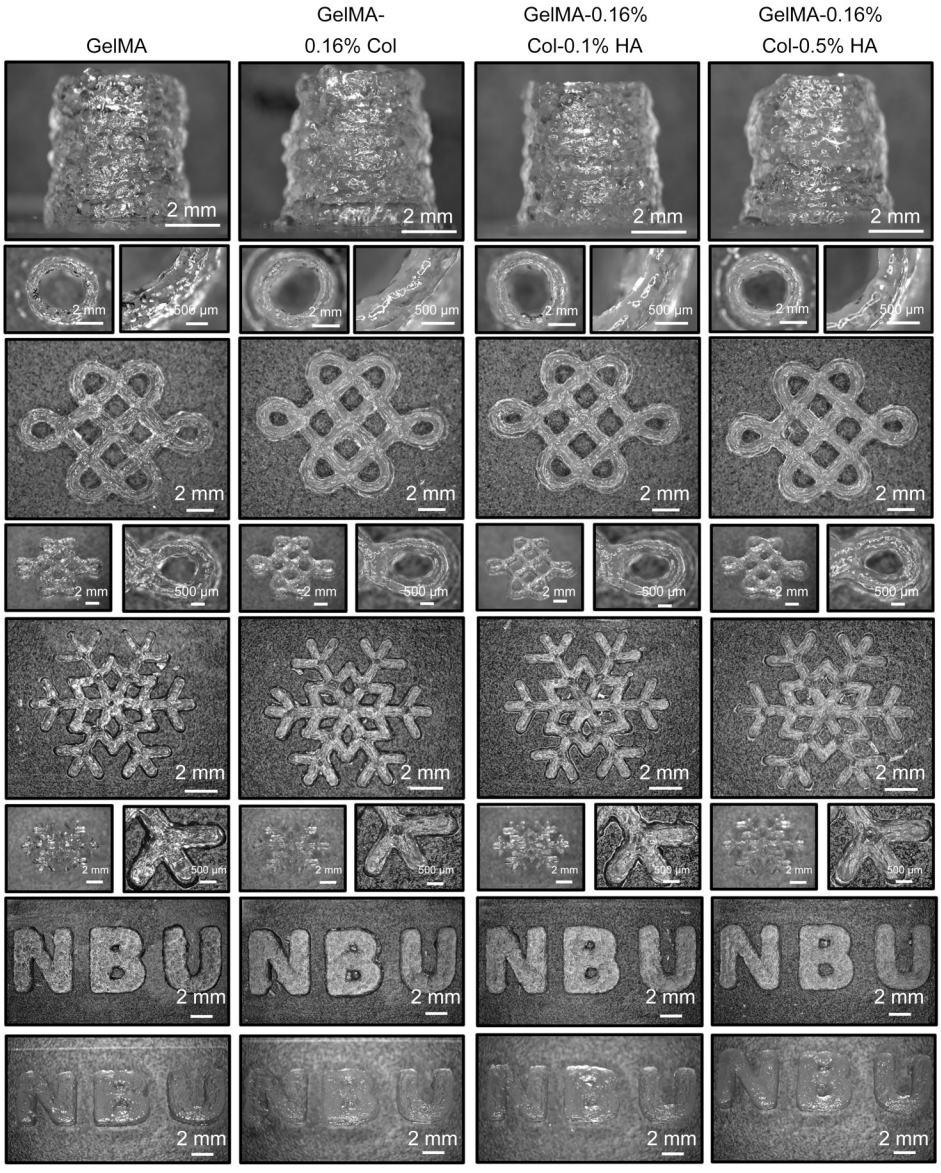

Fig. 5 Complicated structures printed using various concentrations of GelMA-Col-HA bioinks

CCK-8 assays (Fig. 7a). We observed no significant differences between all groups by Day 3, while cells bioprinted in the GelMA-0.16% Col-0.1% HA bioink showed the highest proliferation rate at Days 5 and 7. Next, the cellular viability of MG63 cells after bioprinting was evaluated using live/dead assays. Here, dead cells were colored red (indicated with white arrows), while live cells were green (Fig. 7b). Further quantification showed that cells in all compositions of the hydrogel showed viability levels that were close to 95% (Fig. 7c). This indicated that the inclusion of HA had a limited influence on cellular viability during bioprinting. Next, the morphology of MG63 cells was assessed via phalloidin staining. In general, we found that MG63 cells formed spheroids and showed elongated cellular morphology during culturing (Fig. 7d).

The influence of HA on gene expression in MG63 cells was analyzed by qRT-PCR (Figs. 7e–7p). This analysis included osteogenesis-related genes (i.e., *RUNX2*, *SPP1*, *PTHLH*, and *IBSP*), EMT-related genes (i.e., *SLUG*, *MMP9*, *MMP13*, *MMP2*, *CCL2*, *SNAIL1*, and *VIMENTIN*), and one CSC-related gene (*CD133*). We found that the addition of 0.1% HA significantly upregulated the expression of almost all genes, especially of *IBSP*, *MMP9*, and *CD133* by 3.75-, 3.93-, and 3.53-fold, respectively. However, as the HA concentration increased to 0.5%, we observed a decrease in gene expression. Next, we evaluated the protein expression of SLUG, VIMENTIN, RUNX2, CD44, and CD133 via western blotting. Here, we observed similar results to those for the inclusion of 0.1% HA, where it significantly upregulated the protein expression in general (Figs. 8a–8f). Moreover,

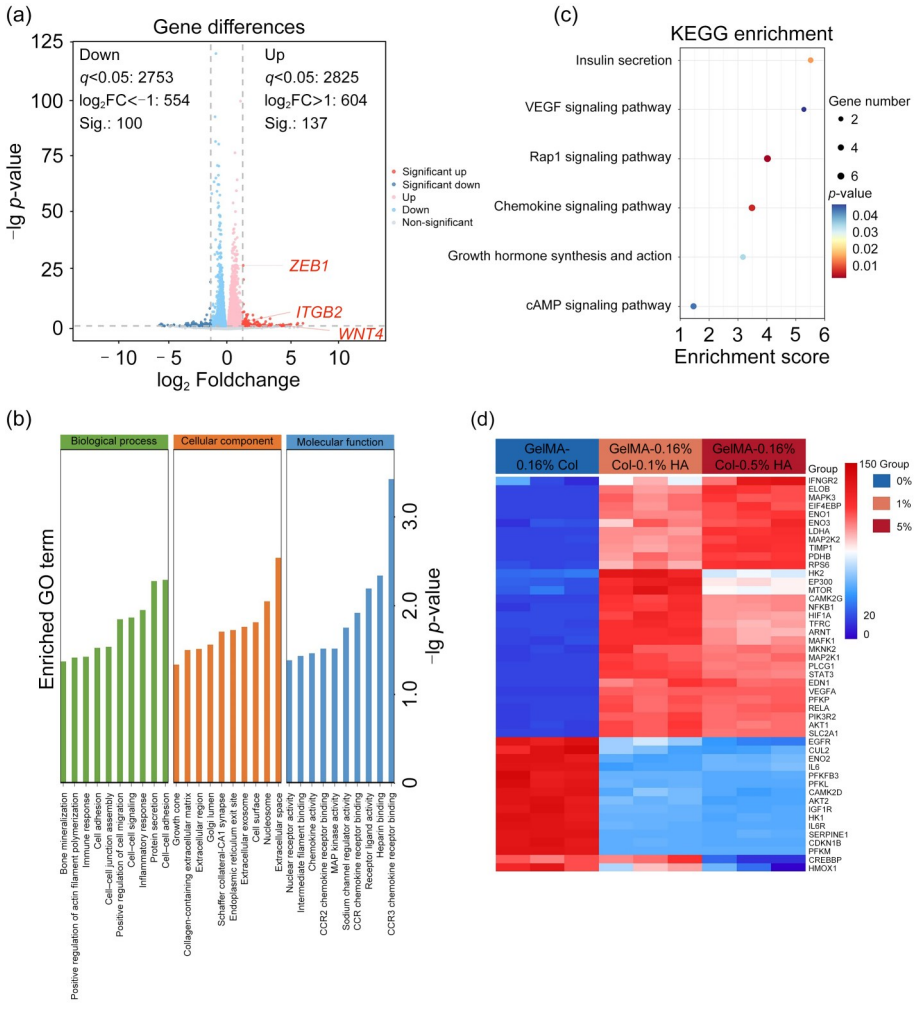

Fig. 6 Transcriptional profiles of osteosarcoma cells in the GelMA-0.16% Col-0.1% HA bioink: (a) volcano plot; (b) GO terms enriched in osteosarcoma cells; (c) KEGG terms enriched in osteosarcoma cells; (d) heat map analysis of the HIF-1α signaling pathway

although the inclusion of 0.5% HA slightly upregulated protein expression compared with the control group, it was still significantly lower than that observed in the 0.1% HA group. Similar results were found in immunofluorescence staining (Figs. 8g–8j). These quantification results showed that MG63 cells in the GelMA-0.16% Col-0.1% HA bioink had higher protein expression in general compared to those in the GelMA-0.16% Col-0.5% HA bioink.

3.6 HA promotes chemoresistance and migration in osteosarcoma cells

To analyze the influence of HA on MG63 cellular migration, we collected cells from bioprinted structures on Day 5 and performed cell scratch assays. As shown in Figs. S5a and S5b (supplementary information), MG63 cells collected from the GelMA-0.16% Col-0.1% HA bioink had a higher migration rate than the other two groups. Next, to analyze the influence of HA on MG63 chemoresistance, hydrogels were cultured with various concentrations of ADM (i.e., at levels of 1 μmol/L and 10 μmol/L) and CDDP (i.e., 10 μmol/L and 100 μmol/L) for 24, 48, and 72 h, after which cellular viability was analyzed by CCK-8 assays. Here, observed viability was normalized to an empty vehicle at the same time point (Figs. 8k–8n). For both ADM and CDDP, MG63 cells bioprinted in the GelMA-0.16% Col bioink showed the lowest cellular viability values for all drug concentrations throughout culturing, indicating that the inclusion of HA improved osteosarcoma chemotherapy resistance. Compared to cells from the GelMA-0.16% Col-0.5% HA bioink, those from the GelMA-0.16% Col-0.1% HA bioink showed relatively high cellular viability values for both drugs after 48 and 72 h; this result was consistent with those of the gene and protein expression analyses.

4 Discussion

Osteosarcoma is a highly aggressive bone cancer with a poor overall prognosis. Traditional in vitro preclinical models, such

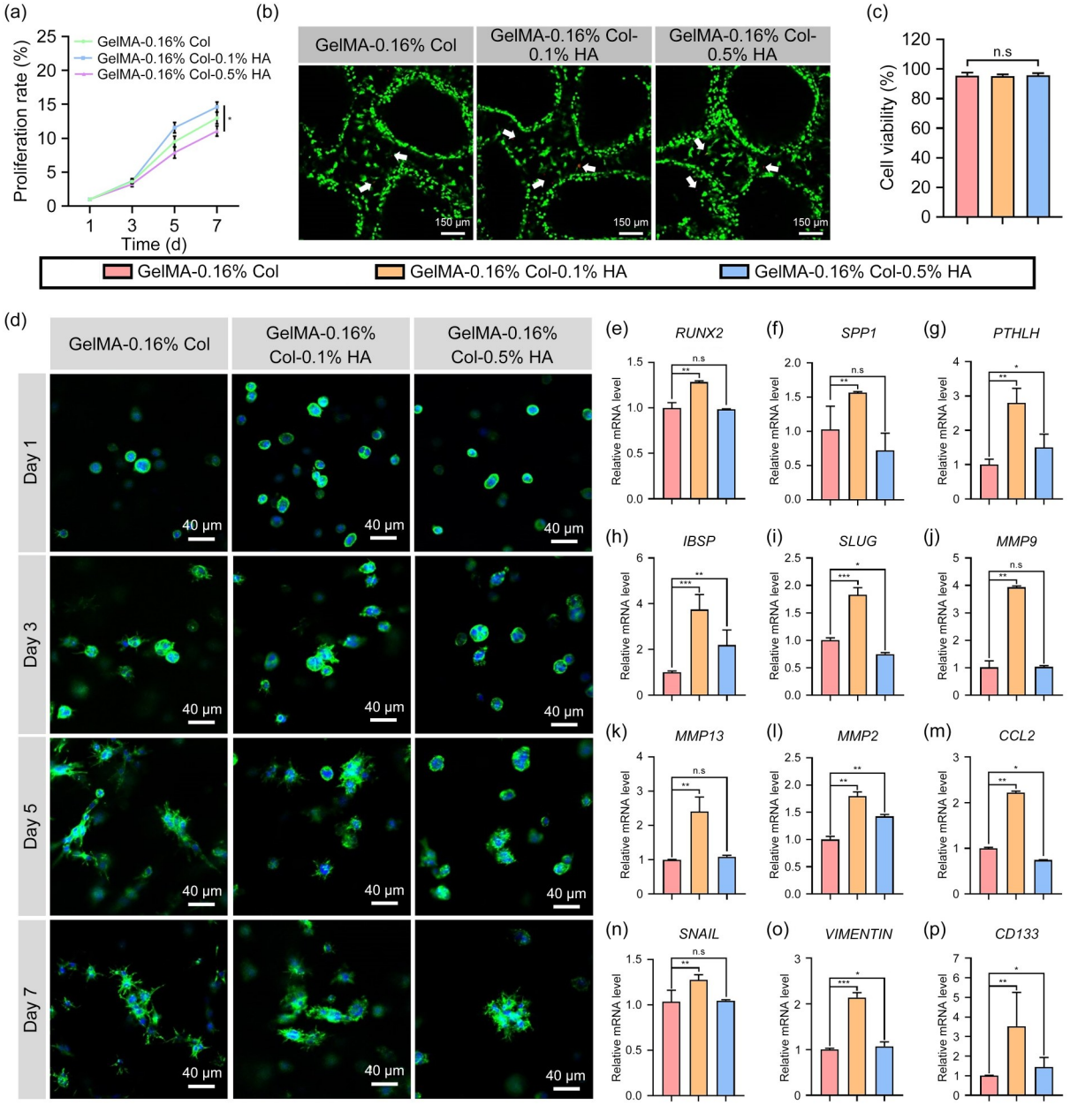

Fig. 7 Biological analysis of osteosarcoma cells in GelMA-Col-HA bioinks: (a) cellular proliferation rates; (b, c) live/dead assay and quantification; (d) cellular morphology of osteosarcoma cells at various time points; (e–p) expression levels of EMT-, CSC-, and osteogenesis-related genes. Data are expressed as mean±standard deviation (n=3); $^{*}p<0.05$, $^{**}p<0.01$, and $^{***}p<0.001$; n.s.: not significant

as monolayer cell cultures, often fail to accurately mimic the TME, which can impede the discovery of effective chemotherapy regimens. In contrast, 3D-bioprinted in vitro tumor models have been developed for several cancers because they can better replicate the spatial, mechanical, and biological complexities of the TME. However, to date, no 3D-bioprinted in vitro osteosarcoma models exist, and no bioink has been specifically designed for this purpose.

GelMA is a commonly used biomaterial due to its rapid gelation time, good printability, and inclusion of RGD sequences that enhance cell adhesion. However, as a derivative of gelatin, GelMA lacks the unique triple-helix structure of collagen [28]. While collagen includes RGD sequences, it also contains Gly-Pro-Hyp (GPO) and Gly-Phe-Hyp (GFO) motifs within its triple helix, and these are crucial for activating signaling pathways and facilitating cell communication. Therefore, in this study we added collagen to GelMA to improve bioactivity and better mimic the ECM composition of the osteosarcoma model. As the collagen concentration increased, the precursors became more viscous due to the more complex polymer network. At the same time, the compressive modulus declined since the collagen molecules

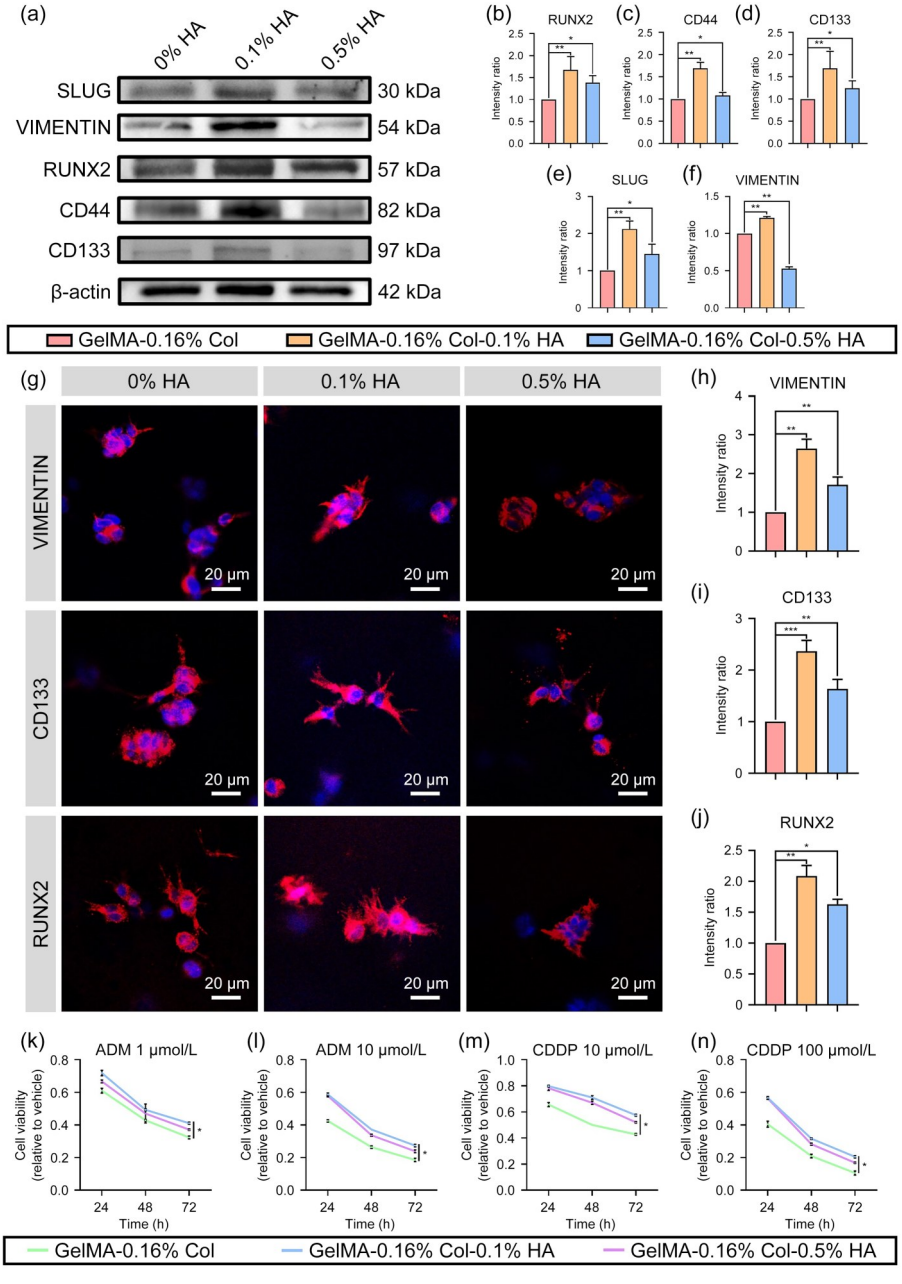

Fig. 8 Protein expression and drug resistance of osteosarcoma cells in GelMA-Col-HA bioinks: (a) western blotting of EMT-, CSC-, and osteogenesis-related markers; (b–f) semi-quantification analysis of western blotting results; (g) immunofluorescence images for VIMENTIN, CD133, and RUNX2; (h–j) semi-quantification analysis of VIMENTIN, CD133, and RUNX2 proteins in immunofluorescence staining; (k–n) ADM and CDDP chemotherapy tests. Data are expressed as mean±standard deviation (n=3); $^{*}p<0.05$, $^{**}p<0.01$, and $^{***}p<0.001$

hindered the photo-crosslinking of GelMA. Overall, MG63 cells cultured in the 3D tumor model demonstrated higher proliferation rates as the collagen concentration increased; this finding was consistent with other studies, which found that collagen had a positive correlation with cellular proliferation in osteosarcoma [29, 30]. Furthermore, collagen may enhance the migration and invasion of osteosarcoma cells by interacting with SOCS5, thereby leading to the suppression of STAT1 expression and activation via ubiquitination and proteasomal degradation [31]. Collagen may also activate the MMP family to mediate osteosarcoma metastasis [9]. In one study, Wei et al. found that collagen can mediate stemness upregulation of osteosarcoma cells via the activation of JAK/STAT3 signaling, thereby strengthening cell proliferation and tumorigenesis [32]. Taken together, these observations were also found in this study—i.e., we found that collagen promoted MG63 metastasis, stemness, and osteogenesis-related gene and protein expression.

HA is abundant in bone [17], and clinical studies have identified a positive correlation between HA concentration and

osteosarcoma development [18], although the underlying mechanism remains poorly understood. Therefore, here we combined various concentrations of HA with GelMA-Col hydrogels to investigate the influence of HA on osteosarcoma cell behavior. RNAseq was then used to analyze differences in transcriptional profiles of osteosarcoma cells following stimulation by HA. ZEB1 is a hallmark transcription factor involved in the cancer cell EMT, and is commonly upregulated in aggressive cancer types; moreover, it is correlated with therapy resistance and metastasis [33, 34]. A recent study also showed that ZEB1 can drive cancer cell ferroptosis sensitivity by manipulating the synthesis of highly oxidizable poly-unsaturated fatty acids [35].

We also found that the HIF-1α signaling pathway was upregulated under HA stimulation. HIF-1α is a transcription factor that is induced in hypoxic microenvironments and is closely associated with tumor progression, angiogenesis, and metastasis [36]. In general, overexpression of HIF-1α has been found in many different tumor types, including human osteosarcoma [37, 38], renal cancer [39], oral squamous cell carcinoma [40], and breast cancer [41], where it correlates significantly with metastasis. HIF-1α has been shown to positively correlate with VEGF [42], a key mediator of tumor angiogenesis and growth [43]. These findings are consistent with our results, which showed that the expression of VEGFA was significantly upregulated in HA samples. The higher chemotherapy resistance of osteosarcoma cells present in the HA bioink may also be affected by the overexpression of HIF-1α, since hypoxic conditions have been shown to increase drug resistance in osteosarcoma cells [44, 45]. To the best of our knowledge, this is the first study to directly demonstrate that there is a positive correlation between HA and HIF-1α in osteosarcoma. This effect may be related to the HA-binding protein KIAA1199; for example, in prostate cancer cells KIAA1199 silencing was found to significantly inhibit HIF-1α expression, angiogenesis, and vasculogenic mimicry in both in vitro and in vivo conditions [46]. It has been found that KIAA1199 has a significantly positive correlation with HIF-1α in pancreatic cancer tissues [47]. A similar phenomenon was observed in our study, in which expression of KIAA1199 mRNA was significantly upregulated in HA samples (Fig. S3e in the supplementary information).

Next, we analyzed EMT- and CSC-related marker expression. As a sarcoma, osteosarcoma arises from mesenchymal cells. However, the importance of EMT in osteosarcoma has been disputed [48, 49]. However, some studies have suggested that the overexpression of EMT-related markers is related to metastasis and contributes to osteosarcoma's poor survival rate [50]. SLUG is a zinc-finger transcription factor that is known to contribute to cell invasion and metastasis in several cancer types [51]. Knockdown of SLUG in osteosarcoma cells was found to result in significantly decreased motility, remodeling of the actin cytoskeleton, loss of cellular protrusions, and significantly smaller tumor size. Therefore, SLUG may be a potential therapeutic target for clinical interventions to combat osteosarcoma [52]. VIMENTIN is an intermediate filament protein that plays a crucial role in modulating cell migration, cell shape, and plasticity. The overexpression of VIMENTIN is observed in many tumor types, and this directly correlates with cancer metastasis and drug resistance [53–55]. In osteosarcomas, increased VIMENTIN expression may be related to more aggressive tumor phenotypes [56]. In addition, higher EMT-related marker expression in the presence of HA may be caused by CD44, a binding protein of HA, since CD44 expression is also strongly correlated with EMT-related markers such as TWIST, SNAIL1, ZEB1, and SLUG [57–59]. CD133 is a key biomarker for the isolation and characterization of cancer stem cells [60], and is significantly correlated with Enneking stage, local recurrence, metastasis, and reduced five-year survival rates in osteosarcoma patients [61]. RUNX2 is a transcription factor critical for osteoblastic differentiation and skeletal morphogenesis. Elevated RUNX2 levels may transcriptionally activate genes mediating tumor progression and metastasis [62], including SPP1 (osteopontin), a phosphorylated protein that is highly expressed in osteosarcomas and is associated with poor prognosis and reduced survival rates [63]. Consistently, in this study both RUNX2 and SPP1 were found to be upregulated in response to HA stimulation. Next, the chemotherapy resistance of osteosarcoma cells was further analyzed using ADM and CDDP at various concentrations. Consistent with our EMT- and CSC-related marker expression results, we observed that osteosarcoma cells had higher drug resistance when in the GelMA-0.16% Col-0.1% HA bioink. Similar results, i.e., where drug resistance increased under HA stimulation, have been found in other cancer cells [64, 65].

Next, we compared the bioinks developed in this study with commercial 3D culture models, including Matrigel and pure collagen. In this experiment, MG63 cells were cultured for five days before being analyzed using immunofluorescence staining, qPCR, and chemotherapy testing (Fig. S6 in the supplementary information). Immunofluorescence staining revealed that MG63 cells cultured in Matrigel and pure collagen exhibited VIMENTIN, CD133, and RUNX2 protein levels that were higher than those in GelMA-0.16% Col but lower than those in GelMA-0.16% Col-0.1% HA. Similar trends were observed in our qPCR results, in which we observed that cells cultured in GelMA-0.16% Col-0.1% HA had the highest expression of cancer-associated genes of all groups, followed by those cultured in Matrigel and pure collagen. Doxorubicin (ADM, 10 μmol/L) and cisplatin (CDDP, 100 μmol/L) were used for chemotherapy tests. Here, MG63 cells cultured in Matrigel and pure collagen displayed comparable drug resistance to GelMA-0.16%

Col-0.5% HA but less resistance than those cultured in GelMA-0.16% Col-0.1% HA. Overall, the bioinks developed in this study offer an improved platform for in vitro culturing of MG63 cells.

In this study, we developed a GelMA-Col-HA composite hydrogel to better replicate the osteosarcoma microenvironment and to investigate the specific impact of HA on osteosarcoma cell behavior. We found that a relatively low concentration of HA significantly promoted osteosarcoma cell growth, metastasis, and drug resistance. Although similar effects were observed at higher HA concentrations, these effects rapidly diminished as the HA concentration increased. Based on the material characterization results, we found almost no physical differences between the GelMA-0.16% Col-0.1% HA and GelMA-0.16% Col-0.5% HA bioinks, except for the compressive modulus. This may play a major role in progression in this study, since the mechanical properties of the ECM are known to play an important role in osteosarcoma progression. In this study, osteosarcoma cells encapsulated within the hydrogel experienced physical restriction due to a higher compressive modulus, and this may have negatively impacted their growth and development. Several other studies have also shown that relatively soft 3D matrices better support osteosarcoma cell proliferation, differentiation, migration, and drug resistance [66–68]. Therefore, despite higher HA concentrations, higher compressive modulus values likely counteracted any promotional effects on osteosarcoma cells.

5 Conclusions

In this study, we developed a composite bioink containing GelMA, collagen, and HA to facilitate the 3D bioprinting of an in vitro tumor model capable of simulating the ECM composition of the osteosarcoma microenvironment. Moreover, we investigated the influence of HA on cellular behavior. We found that HA significantly promoted osteosarcoma cell growth and enhanced chemoresistance, and was accompanied by upregulated expression of EMT- and CSC-related markers. In addition, we found a positive correlation between HA and the HIF-1α signaling pathway; to our knowledge this is the first study to demonstrate this connection. Overall, the GelMA-Col-HA bioink developed in this study provides a realistic 3D model for studying osteosarcoma and may be an appropriate preclinical in vitro model of osteosarcoma for drug screening.

Supplementary Information The online version contains supplementary material available at https://doi.org/10.1631/bdm.2400390.

Acknowledgements This work was supported by the Natural Science Foundation of Zhejiang Province (No. TGY24E050004), the Ningbo Major Research and Development Plan Project (No. 2024Z208), the National Natural Science Foundation of China (No. 12202387), the Ningbo Health Technology Project (No. 2023Y16), and the Natural Science Foundation of Ningbo (No. 2022J212).

Author contributions HYZ: methodology, investigation, formal analysis, and writing—original draft; MBW: methodology and investigation; ZKD: methodology and investigation; WS: validation; HKJ: validation; KXC: validation; YBW: formal analysis and funding acquisition; EXY: formal analysis and funding acquisition; YYH: writing—original draft; QHS: conceptualization and writing—review & editing; KLX: conceptualization, methodology, supervision, funding acquisition, and writing—review & editing.

Declarations

Conflict of interest The authors declare that they have no conflict of interest.

Ethical approval This article does not contain any studies with human or animal subjects performed by any of the authors.

Data availability The data that support the findings of this study are available from the corresponding authors upon reasonable request.

References

1. Misaghi A, Goldin A, Awad M et al (2018) Osteosarcoma: a comprehensive review. SICOT J 4:12. https://doi.org/10.1051/sicotj/2017028
2. Shin SH, Jeong HJ, Han I et al (2013) Osteosarcoma and chondrosarcoma of the shoulder: site-specific comparative analysis. Orthopedics 36(2):e179–e185. https://doi.org/10.3928/01477447-20130122-20
3. Guo J, Reddick WE, Glass JO et al (2012) Dynamic contrast-enhanced magnetic resonance imaging as a prognostic factor in predicting event-free and overall survival in pediatric patients with osteosarcoma. Cancer 118(15):3776–3785. https://doi.org/10.1002/cncr.26701
4. Hynes RO (2009) The extracellular matrix: not just pretty fibrils. Science 326(5957):1216–1219. https://doi.org/10.1126/science.1176009
5. Lewis DI (2019) Animal experimentation: implementation and application of the 3Rs. Emerg Top Life Sci 3(6):675–679. https://doi.org/10.1042/ETLS20190061
6. Rimann M, Laternser S, Gvozdenovic A et al (2014) An in vitro osteosarcoma 3D microtissue model for drug development. J Biotechnol 189:129–135. https://doi.org/10.1016/j.jbiotec.2014.09.005
7. Monteiro MV, Gaspar VM, Ferreira LP et al (2020) Hydrogel 3D in vitro tumor models for screening cell aggregation mediated drug response. Biomater Sci 8(7):1855–1864. https://doi.org/10.1039/C9BM02075F
8. Neufurth M, Wang XH, Schröder HC et al (2014) Engineering a morphogenetically active hydrogel for bioprinting of bioartificial tissue derived from human osteoblast-like SaOS-2 cells. Biomaterials 35(31):8810–8819. https://doi.org/10.1016/j.biomaterials.2014.07.002
9. Elenjord R, Allen JB, Johansen HT et al (2009) Collagen I regulates matrix metalloproteinase-2 activation in osteosarcoma cells independent of S100A4. FEBS J 276(18):5275–5286. https://doi.org/10.1111/j.1742-4658.2009.07223.x
10. Thai VL, Griffin KH, Thorpe SW et al (2021) Tissue engineered platforms for studying primary and metastatic neoplasm behavior in bone. J Biomech 115:110189.

https://doi.org/10.1016/j.jbiomech.2020.110189
11. Xu KL, Huang YY, Wu MB et al (2023) 3D bioprinting of multicellular tumor microenvironment for prostate cancer metastasis. Biofabrication 15(3):035020. https://doi.org/10.1088/1758-5090/acd960
12. Wu MB, Zhou HY, Hu JY et al (2024) Decellularized porcine kidney-incorporated hydrogels for cell-laden bioprinting of renal cell carcinoma model. Int J Bioprinting 10(1):1413. https://doi.org/10.36922/ijb.1413
13. Mao SS, He JY, Zhao Y et al (2020) Bioprinting of patient-derived in vitro intrahepatic cholangiocarcinoma tumor model: establishment, evaluation and anti-cancer drug testing. Biofabrication 12(4):045014. https://doi.org/10.1088/1758-5090/aba0c3
14. Xie FH, Sun LJ, Pang Y et al (2021) Three-dimensional bioprinting of primary human hepatocellular carcinoma for personalized medicine. Biomaterials 265:120416. https://doi.org/10.1016/j.biomaterials.2020.120416
15. Shan Y, Pang MC, Wang LQ et al (2024) Increased stiffness of extracellular matrix enhanced chemoresistance in 3D-bioprinted ovarian cancer model. Int J Bioprinting:1673. https://doi.org/10.36922/ijb.1673
16. Kunz P, Sähr H, Lehner B et al (2016) Elevated ratio of MMP2/MMP9 activity is associated with poor response to chemotherapy in osteosarcoma. BMC Cancer 16:223. https://doi.org/10.1186/s12885-016-2266-5
17. Liang JR, Jiang DH, Noble PW (2016) Hyaluronan as a therapeutic target in human diseases. Adv Drug Deliv Rev 97:186–203. https://doi.org/10.1016/j.addr.2015.10.017
18. Toole BP (2004) Hyaluronan: from extracellular glue to pericellular cue. Nat Rev Cancer 4(7):528–539. https://doi.org/10.1038/nrc1391
19. Nishida Y, Knudson W, Knudson CB et al (2005) Antisense inhibition of hyaluronan synthase-2 in human osteosarcoma cells inhibits hyaluronan retention and tumorigenicity. Exp Cell Res 307(1):194–203. https://doi.org/10.1016/j.yexcr.2005.03.026
20. Hosono K, Nishida Y, Knudson W et al (2007) Hyaluronan oligosaccharides inhibit tumorigenicity of osteosarcoma cell lines MG-63 and LM-8 in vitro and in vivo via perturbation of hyaluronan-rich pericellular matrix of the cells. Am J Pathol 171(1):274–286. https://doi.org/10.2353/ajpath.2007.060828
21. Zhu MX, Wang YY, Ferracci G et al (2019) Gelatin methacryloyl and its hydrogels with an exceptional degree of controllability and batch-to-batch consistency. Sci Rep 9(1):6863. https://doi.org/10.1038/s41598-019-42186-x
22. Chow T, Wutami I, Lucarelli E et al (2021) Creating in vitro three-dimensional tumor models: a guide for the biofabrication of a primary osteosarcoma model. Tissue Eng Part B Rev 27(5): 514–529. https://doi.org/10.1089/ten.teb.2020.0254
23. Wang ML, Xu NY, Tang RZ et al (2022) A 3D-printed scaffold-based osteosarcoma model allows to investigate tumor phenotypes and pathogenesis in an in vitro bone-mimicking niche. Mater Today Bio 15:100295. https://doi.org/10.1016/j.mtbio.2022.100295
24. Delgrosso E, Scocozza F, Cansolino L et al (2023) 3D bioprinted osteosarcoma model for experimental boron neutron capture therapy (BNCT) applications: preliminary assessment. J Biomed Mater Res B Appl Biomater 111(8):1571–1580. https://doi.org/10.1002/jbm.b.35255
25. Sawyer SW, Oest ME (2016) Behavior of encapsulated Saos-2 cells within gelatin methacrylate hydrogels. J Tissue Sci Eng 7(2): 1000173. https://doi.org/10.4172/2157-7552.1000173
26. Jansen LE, Birch NP, Schiffman JD et al (2015) Mechanics of intact bone marrow. J Mech Behav Biomed Mater 50:299–307. https://doi.org/10.1016/j.jmbbm.2015.06.023
27. Chen XD, Dusevich V, Feng JQ et al (2007) Extracellular matrix made by bone marrow cells facilitates expansion of marrow-derived mesenchymal progenitor cells and prevents their differentiation into osteoblasts. J Bone Miner Res 22(12):1943–1956. https://doi.org/10.1359/jbmr.070725
28. Shi HM, Li Y, Xu KL et al (2023) Advantages of photo-curable collagen-based cell-laden bioinks compared to methacrylated gelatin (GelMA) in digital light processing (DLP) and extrusion bioprinting. Mater Today Bio 23:100799. https://doi.org/10.1016/j.mtbio.2023.100799
29. Cui JC, Dean D, Hornicek FJ et al (2020) The role of extracelluar matrix in osteosarcoma progression and metastasis. J Exp Clin Cancer Res 39(1):178. https://doi.org/10.1186/s13046-020-01685-w
30. Mullick P, Das G, Aiyagari R (2022) 2-Dodecylmalonic acid-mediated synthesis of mineralized hydroxyapatite amicable for bone cell growth on orthopaedic implant. J Colloid Interface Sci 608:2298–2309. https://doi.org/10.1016/j.jcis.2021.10.157
31. Zhang Y, Liu ZY, Yang X et al (2021) H3K27 acetylation activated-COL6A1 promotes osteosarcoma lung metastasis by repressing STAT1 and activating pulmonary cancer-associated fibroblasts. Theranostics 11(3):1473–1492. https://doi.org/10.7150/thno.51245
32. Wei DQ, Li C, Ye JW et al (2020) Extracellular collagen mediates osteosarcoma progression through an integrin α2β1/JAK/STAT3 signaling pathway. Cancer Manag Res 12:12067–12075. https://doi.org/10.2147/CMAR.S273466
33. Brabletz S, Schuhwerk H, Brabletz T et al (2021) Dynamic EMT: a multi-tool for tumor progression. EMBO J 40(18):e108647. https://doi.org/10.15252/embj.2021108647
34. Nieto MA, Huang RY, Jackson RA et al (2016) EMT: 2016. Cell 166(1):21–45. https://doi.org/10.1016/j.cell.2016.06.028
35. Schwab A, Rao ZG, Zhang J et al (2024) Zeb1 mediates EMT/plasticity-associated ferroptosis sensitivity in cancer cells by regulating lipogenic enzyme expression and phospholipid composition. Nat Cell Biol 26(9):1470–1481. https://doi.org/10.1038/s41556-024-01464-1
36. Nepal M, Choi HJ, Choi BY et al (2012) Anti-angiogenic and anti-tumor activity of Bavachinin by targeting hypoxia-inducible factor-1α. Eur J Pharmacol 691(1–3):28–37. https://doi.org/10.1016/j.ejphar.2012.06.028
37. Yang QC, Zeng BF, Dong Y et al (2007) Overexpression of hypoxia-inducible factor-1α in human osteosarcoma: correlation with clinicopathological parameters and survival outcome. Jpn J Clin Oncol 37(2):127–134. https://doi.org/10.1093/jjco/hyl137
38. Chen WL, Feng HJ, Li HG (2008) Expression and significance of hypoxemia-inducible factor-1α in osteosarcoma of the jaws. Oral Surg Oral Med Oral Pathol Oral Radiol Endod 106(2): 254–257. https://doi.org/10.1016/j.tripleo.2008.01.029
39. Staller P, Sulitkova J, Lisztwan J et al (2003) Chemokine receptor CXCR4 downregulated by von Hippel–Lindau tumour suppressor pVHL. Nature 425(6955):307–311. https://doi.org/10.1038/nature01874
40. Ishikawa T, Nakashiro KI, Klosek SK et al (2009) Hypoxia enhances CXCR4 expression by activating HIF-1 in oral squamous cell carcinoma. Oncol Rep 21(3):707–712. https://doi.org/10.3892/or_00000275

41. Cronin PA, Wang JH, Redmond HP (2010) Hypoxia increases the metastatic ability of breast cancer cells via upregulation of CXCR4. BMC Cancer 10:225. https://doi.org/10.1186/1471-2407-10-225
42. Mizobuchi H, García-Castellano JM, Philip S et al (2008) Hypoxia markers in human osteosarcoma: an exploratory study. Clin Orthop Relat Res 466(9):2052–2059. https://doi.org/10.1007/s11999-008-0328-y
43. Salimath B, Marmé D, Finkenzeller G (2000) Expression of the vascular endothelial growth factor gene is inhibited by p73. Oncogene 19(31):3470–3476. https://doi.org/10.1038/sj.onc.1203672
44. Roncuzzi L, Pancotti F, Baldini N (2014) Involvement of HIF-1α activation in the doxorubicin resistance of human osteosarcoma cells. Oncol Rep 32(1):389–394. https://doi.org/10.3892/or.2014.3181
45. Adamski J, Price A, Dive C et al (2013) Hypoxia-induced cytotoxic drug resistance in osteosarcoma is independent of HIF-1alpha. PLoS ONE 8(6):e65304. https://doi.org/10.1371/journal.pone.0065304
46. Luo YW, Yang ZH, Yu Y et al (2022) HIF1α lactylation enhances KIAA1199 transcription to promote angiogenesis and vasculogenic mimicry in prostate cancer. Int J Biol Macromol 222:2225–2243. https://doi.org/10.1016/j.ijbiomac.2022.10.014
47. Oba T, Sato N, Adachi Y et al (2021) Hypoxia increases KIAA1199/CEMIP expression and enhances cell migration in pancreatic cancer. Sci Rep 11(1):18193. https://doi.org/10.1038/s41598-021-97752-z
48. Sannino G, Marchetto A, Kirchner T et al (2017) Epithelial-to-mesenchymal and mesenchymal-to-epithelial transition in mesenchymal tumors: a paradox in sarcomas? Cancer Res 77(17): 4556–4561. https://doi.org/10.1158/0008-5472.CAN-17-0032
49. Kahlert UD, Joseph JV, Kruyt FAE (2017) EMT- and MET-related processes in nonepithelial tumors: importance for disease progression, prognosis, and therapeutic opportunities. Mol Oncol 11(7): 860–877. https://doi.org/10.1002/1878-0261.12085
50. Hinton K, Kirk A, Paul P et al (2023) Regulation of the epithelial to mesenchymal transition in osteosarcoma. Biomolecules 13(2):398. https://doi.org/10.3390/biom13020398
51. Ganesan R, Mallets E, Gomez-Cambronero J (2016) The transcription factors Slug (SNAI2) and Snail (SNAI1) regulate phospholipase D (PLD) promoter in opposite ways towards cancer cell invasion. Mol Oncol 10(5):663–676. https://doi.org/10.1016/j.molonc.2015.12.006
52. Sharili AS, Allen S, Smith K et al (2013) Snail2 promotes osteosarcoma cell motility through remodelling of the actin cytoskeleton and regulates tumor development. Cancer Lett 333(2):170–179. https://doi.org/10.1016/j.canlet.2013.01.027
53. Shang YJ, Li ZY, Li H et al (2013) TIM-3 expression in human osteosarcoma: correlation with the expression of epithelial-mesenchymal transition-specific biomarkers. Oncol Lett 6(2): 490–494. https://doi.org/10.3892/ol.2013.1410
54. Satelli A, Li SL (2011) Vimentin in cancer and its potential as a molecular target for cancer therapy. Cell Mol Life Sci 68(18): 3033–3046. https://doi.org/10.1007/s00018-011-0735-1
55. Li M, Zhang BG, Sun BC et al (2010) A novel function for vimentin: the potential biomarker for predicting melanoma hematogenous metastasis. J Exp Clin Cancer Res 29(1):109. https://doi.org/10.1186/1756-9966-29-109
56. Amaral CB, Leite JDS, Fonseca ABM et al (2018) Vimentin, osteocalcin and osteonectin expression in canine primary bone tumors: diagnostic and prognostic implications. Mol Biol Rep 45(5): 1289–1296. https://doi.org/10.1007/s11033-018-4285-6
57. Bhat-Nakshatri P, Appaiah H, Ballas C et al (2010) SLUG/SNAI2 and tumor necrosis factor generate breast cells with $CD44^{+}$/CD24− phenotype. BMC Cancer 10:411. https://doi.org/10.1186/1471-2407-10-411
58. Marín-Aguilera M, Codony-Servat J, Reig Ò et al (2014) Epithelial-to-mesenchymal transition mediates docetaxel resistance and high risk of relapse in prostate cancer. Mol Cancer Ther 13(5):1270–1284. https://doi.org/10.1158/1535-7163.MCT-13-0775
59. Wu KJ, Ning ZY, Zeng J et al (2013) Silibinin inhibits β-catenin/ZEB1 signaling and suppresses bladder cancer metastasis via dual-blocking epithelial–mesenchymal transition and stemness. Cell Signal 25(12):2625–2633. https://doi.org/10.1016/j.cellsig.2013.08.028
60. Li Z (2013) CD133: a stem cell biomarker and beyond. Exp Hematol Oncol 2(1):17. https://doi.org/10.1186/2162-3619-2-17
61. Xu N, Kang YJ, Wang WC et al (2020) The prognostic role of CD133 expression in patients with osteosarcoma. Clin Exp Med 20(2):261–267. https://doi.org/10.1007/s10238-020-00607-6
62. Villanueva F, Araya H, Briceño P et al (2018) The cancer-related transcription factor RUNX2 modulates expression and secretion of the matricellular protein osteopontin in osteosarcoma cells to promote adhesion to endothelial pulmonary cells and lung metastasis. J Cell Physiol 234:13659–13679. https://doi.org/10.1002/jcp.28046
63. Zhang ZM, Liu BF, Lin ZJ et al (2024) SPP1 could be an immunological and prognostic biomarker: from pan-cancer comprehensive analysis to osteosarcoma validation. FASEB J 38(14):e23783. https://doi.org/10.1096/fj.202400622RR
64. Liu Z, Hou P, Fang J et al (2024) Hyaluronic acid metabolism and chemotherapy resistance: recent advances and therapeutic potential. Mol Oncol 18(9):2087–2106. https://doi.org/10.1002/1878-0261.13551
65. Florczyk SJ, Wang K, Jana S et al (2013) Porous chitosan-hyaluronic acid scaffolds as a mimic of glioblastoma microenvironment ECM. Biomaterials 34(38):10143–10150. https://doi.org/10.1016/j.biomaterials.2013.09.034
66. Lin YX, Yuan K, Yang YQ et al (2023) Osteosarocma progression in biomimetic matrix with different stiffness: insights from a three-dimensional printed gelatin methacrylamide hydrogel. Int J Biol Macromol 252:126391. https://doi.org/10.1016/j.ijbiomac.2023.126391
67. Li S, Bai HX, Chen XY et al (2020) Soft substrate promotes osteosarcoma cell self-renewal, differentiation, and drug resistance through miR-29b and its target protein Spin 1. ACS Biomater Sci Eng 6(10):5588–5598. https://doi.org/10.1021/acsbiomaterials.0c00816
68. Kundu B, Bastos AF, Brancato V et al (2019) Mechanical property of hydrogels and the presence of adipose stem cells in tumor stroma affect spheroid formation in the 3D osteosarcoma model. ACS Appl Mater Interfaces 11(16):14548–14559. https://doi.org/10.1021/acsami.8b22724